On Predistortion Filtering for Switched Beamforming With Phased-Array Antennas

Derek Caudill, Jack Chuang, Camillo Gentile, and Sung Yun Jun
Communications Technology Laboratory
National Institute of Standards and Technology (NIST), USA
camillo.gentile@nist.gov

***Abstract*—In recent work on channel sounding, we proposed switching the antennas of phased arrays and beamforming in postprocessing – what we coined *switched beamforming* – instead of scanning beams through analog beamforming – what the arrays are designed for. Not only is switched beamforming orders of magnitude quicker than analog beamforming, it also synthesizes beam patterns that are quasi-ideal. In the same work, we proposed predistortion filtering to calibrate the channel sounder by designing a separate filter for each of the switched antennas. It was later found that the design neglects the mutual leakage between the antennas on the printed circuit board. In this paper, we propose an improved design that considers all antennas collectively to account for the leakage. Not only does it increase the peak-to-sidelobe ratio of the channel impulse response by up to 21 dB, the response is also stable across the range of beamformed angles.**

***Index Terms*—5G, 28.5 GHz, calibration, channel sounder, channel sounding, millimeter-wave, mmWave, propagation.**

I. Introduction

NextG wireless systems [1] will exploit swaths of available bandwidth in the millimeter-wave and sub-terahertz regimes to deliver gigabits/s data rates, but to combat the greater pathloss in those regimes and the greater noise inherent to gigahertz bandwidths, directional antennas – by virtue of their high gain – will be employed to boost the received power [2]-[5]. For the same reasons, NextG channel sounders will employ directional antennas. Phased arrays [6]-[10] are the antennas of choice thanks to their electronic steerability to quickly scan beams in angle and their flexibility to shape the beam pattern for enhanced sidelobe suppression.

Phased-array antennas are designed for analog beamforming, *i.e.* programming the (complex) analog weights of the antennas by controlling the amplifiers and phase shifters on the printed circuit board to synthesize electronic beams. Analog beamforming, however, has two major drawbacks: 1. Scanning the beam involves reprogramming the analog weights at each steer angle, which is time consuming; 2. The analog weights have finite precision, limiting the shape of the beam pattern synthesized, and moreover the ability to compensate for the hardware imperfections of the board through fine weight calibration, lending to beams that are asymmetrical, have poor sidelobe suppression, double lobes, etc. This in turn degrades estimation of the channel properties.

In recent work, we proposed *switched beamforming* [11]: rather than scanning the beam sequentially through analog beamforming, we switch the antennas sequentially and beamform in postprocessing by applying digital weights. This avoids the time-consuming reprogramming of the analog weights and, since the digital weights effectively have infinite precision, the beam pattern can be shaped to quasi-ideal. In the same work, we proposed calibrating the channel sounder through predistortion filtering. A separate filter was designed for each of the switched antennas. While significantly improving the peak-to-sidelobe ratio of the channel impulse response with respect to no filter at all, because the filter was designed separately for every antenna, the leakage between the antennas on the printed circuit was not accounted for.

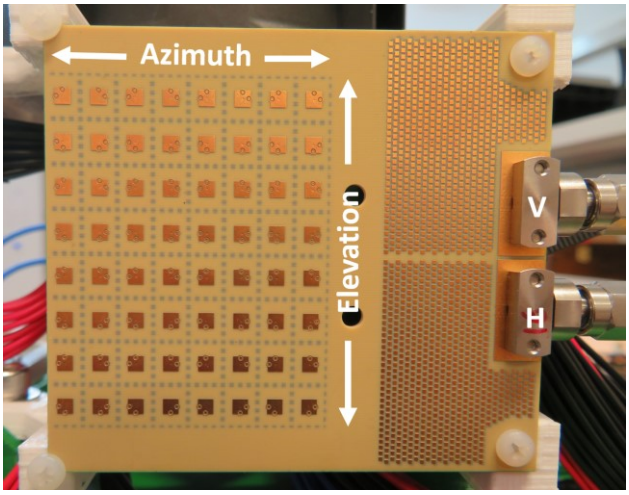

Figure 1. 28.5 GHz 8 x 8 phased-array antenna printed circuit board. Each of the 64 elements features stacked vertically and horizontally polarized microstrip antennas with a separate port per polarization. The beams that the array synthesizes are steerable in both azimuth and elevation.

To account for the leakage between the antennas, in this paper we propose an improved design. Rather than designing a separate predistortion filter for each of the antennas, the design considers all antennas collectively. Not only did it increase peak-to-sidelobe ratio by up to 21 dB, it was stable across the range of different beamforming angles. The rest of paper is developed as follows: Section II describes our 28.5 GHz phased-array channel sounder and the switched beamforming technique. Section III describes our original predistortion design, followed by our improved design in Section IV. The last section provides guidance for future work.

II. Channel Sounding

In this section, we provide an overview of our 28.5 GHz phased-array channel sounder and how switched beamforming is implemented. Complete details on both can be found in [11].

A. 28.5 GHz Phased-Array Channel Sounder

Our channel sounder features switchable vertical (V) and horizontal (H) polarized directional antennas at the transmitter (T), and at the receiver (R) an 8 x 8 phased array of stacked V and H microstrip patch antennas on a printed circuit board [12]. The R array is shown in Fig. 1, where the antennas are spaced roughly at half wavelength at the 28.5 GHz center frequency of the system. The magnitude and phase of each antenna – what we refer to collectively as its (complex) analog weight – are independently programmable through a serial peripheral interface (SPI), with 8-bit magnitude precision and 6-bit phase precision. (The SPI port is on the back of the array.) The SPI also features a channel select register to toggle each antenna on/off via its DC amplifier, to allow for separate antenna calibration. The antennas are fed through a Wilkinson power combiner to a single shared radio frequency (RF) port per polarization; the cross-polarization rejection between the ports is 35 dB. By programming the analog weights, the array is designed to synthesize an electronically steerable beam that can be scanned ±45° in azimuth and ±25° in elevation.

An arbitrary waveform generator (AWG) at T generates a BPSK-modulated M-ary pseudorandom-noise (PN) code of 2047 chips (33 dB processing gain) with 0.5 ns chip duration (2 GHz bandwidth). The code is generated at an intermediate frequency (IF) of 4 GHz, is upconverted to 28.5 GHz through an on-board mixer, and switched through the V and H antennas sequentially. The complex receiver power at the V and H ports of the array is downconverted back to IF, where it is sampled directly at a rate of 16 gigasamples/s via a digitizer, as opposed to on-the-fly correlation [13]. Finally, the sampled signal is correlated with the known PN code in postprocessing to generate a complex channel impulse response (CIR) $\hat{y}(\tau)$ in the delay domain τ.

B. Switched Beamforming

Phased-array antennas – including ours – are designed to synthesize an electronic beam by coherently phasing the antennas through analog beamforming, by programming their analog weights through the SPI controller. The beam is scanned in angle electronically by reprogramming the weights each time. The drawback of *beam scanning* is that programming is time consuming: for our arrays it takes 3.5 µs to program each antenna, or equivalently 3.5 µs x 64 = 224 µs to program a beam across all 64 antennas. To obtain the best angular estimation possible, it is desirable to scan the beam at the finest angle possible, which for our arrays is 1.8° in azimuth and 1.4° in elevation given the 6-bit phase precision. This translates to scanning 50 x 36 = 1800 beams within the ±45° azimuth and ±25° elevation field-of-view, requiring 224 µs x 1800 = 403.2 ms, much beyond the targeted maximum channel sweep duration of a few milliseconds [2][14].

Instead of beam scanning, we implement *antenna switching* by exploiting the channel select register to switch each antenna on one at a time, requiring 3.5 µs each. A single code is transmitted per antenna through time multiplexing, requiring 3.5 µs x 64 = 224 µs for the total sweep, 1800 times faster than beam scanning. Once the antenna responses are sampled, beams are synthesized in postprocessing through switched beamforming. Critically, the beams can be scanned *at any angle* without changing the channel sweep duration. After sampling and correlation, the scan yields the antenna response $\hat{\boldsymbol{y}}(\tau)$, which is row vector of 64 CIRs.

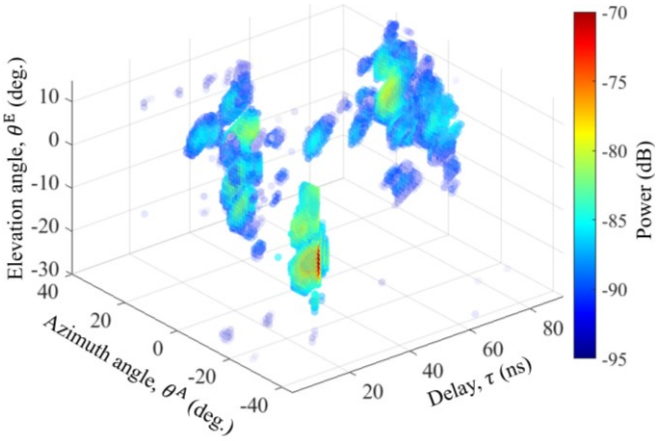

Figure 2. Power angle-delay profile $PADP(\theta^{\mathrm{A}}, \theta^{\mathrm{E}}, \tau)$ for an example measurement.

As in analog beamforming, switched beamforming is implemented by applying complex weights to the array antennas – specifically to the antenna responses – to synthesize beams in postprocessing. The ideal digital weights for steering towards 3D angle $\boldsymbol{\theta} = [\theta^{\mathrm{A}}\ \theta^{\mathrm{E}}]$, where A denotes azimuth and E elevation, are stored compactly in the 64-length row steering vector [15]:

$$\boldsymbol{s}(\boldsymbol{\theta}) = e^{j\frac{2\pi}{\lambda}(\cos\theta^{\mathrm{A}}\cdot\cos\theta^{\mathrm{E}},\ \sin\theta^{\mathrm{A}}\cdot\cos\theta^{\mathrm{E}},\ \sin\theta^{\mathrm{E}})\cdot\boldsymbol{X}}, \qquad (1)$$

where $\boldsymbol{X}$ is a 3 x 64 matrix of the 3D positions of the antennas on the board.

Although the actual steering is implemented through digital weights, the analog weights must nevertheless be programmed to some nominal values; once programmed, they need not be reprogrammed. Their magnitude is set equal to the maximum value of the register to maximize the radiated power, and their phase is set equal to 0 radians. Given the hardware imperfections of the board and the finite precision of the analog weights, their actual values will deviate from the nominal values across the array. To compensate for this, the actual values are reset precisely to the nominal values by modifying the digital weights from their ideal values – that is – from the ideal steering vector $\boldsymbol{s}(\boldsymbol{\theta})$ in (1) to the calibrated steering vector $\hat{\boldsymbol{s}}(\boldsymbol{\theta})$. How this is achieved is beyond the scope of this paper but is discussed in detail in [11]. The antenna response is then beamformed into a power angle-delay profile:

$$PADP(\boldsymbol{\theta}, \tau) = \left|\hat{\boldsymbol{s}}(\boldsymbol{\theta}) \cdot \hat{\boldsymbol{y}}(\tau)^{\dagger}\right|^2, \qquad (2)$$

where † is the conjugate transpose operator. A power angle-delay profile for an example measurement in the field is shown in Fig. 2.

While reducing the channel sweep duration by orders of magnitude is a significant advantage of switched beamforming, the other significant advantage is the accuracy

that is gained from the effectively infinite precision of digital weights compared to the 8-bit magnitude and 6-bit phase precision of the analog weights. That is what enables beam scanning at any angle, pivotal to the successful implementation of super-resolution algorithms [16]-[21] for extracting discrete paths from the power angle-delay profile. But where infinite precision matters most is in the fine calibration of the digital weights to synthesize quasi-ideal beams patterns [11].

III. Original Predistortion Filter

So that the properties of the discrete paths extracted from the power angle-delay profile reflect the channel alone – not the channel plus the channel sounder – all traces of the equipment must be decoupled from the measurements through calibration. In early work [22], we implemented postdistortion filtering, in which the received response is calibrated. Since, we have implemented predistortion filtering [11][23]-[25], in which the ideal PN code – the probing signal – is calibrated before it is transmitted. The latter is preferable because it can be applied at a greater signal-to-noise level (at T) to avoid boosting the noise level (at R). Once designed, it is the predistorted code that is generated by the AWG, not the ideal code (although the ideal code is still used for correlation at R). Given the high cross-polarization rejection of the boards (35 dB), any cross-polarization leakage is ignored and the filters are designed separately for V and H. Our original predistortion filter design from [11] is discussed in this section.

In the conventional *back-to-back* design method [23], the T and R RF front ends are disconnected from the antennas and reconnected through a waveguide with known attenuation A; the antennas are calibrated in a separate step. The *over-the-air* (OTA) method [24][25] that we implement here is similar, but the whole RF chain – the RF front ends plus the antennas on the printed circuit board – is accounted for in a single step since the antennas cannot be disconnected. The OTA method exploits the line-of-sight (LoS) path between the T and R. Specifically, the T and R were placed in an anechoic chamber, separated by precisely 3 m, and their antennas were pointed towards each other, with the boresight of the T antennas aligned with the normal of the R array.

For simplicity, the predistortion filter design is presented in the frequency domain instead of the delay domain, where $\widehat{\boldsymbol{Y}}(f)$ is the Fourier transform of $\widehat{\boldsymbol{y}}(\tau)$. Rather than generating the ideal PN code $p(f)$, the AWG generates the predistorted codes $p(f)\cdot\boldsymbol{W}(f)$ – one for each of the antennas – where $\boldsymbol{W}(f)$ is a row vector of 64 filters. The antenna frequency response at R can be expressed as

$$\widehat{\boldsymbol{Y}}(f) = P(f)\cdot\boldsymbol{W}(f)\odot H^{\mathrm{T}}(f)\cdot\boldsymbol{H}(f)\odot\boldsymbol{H}^{\mathrm{R}}(f)+\boldsymbol{N}(f), \quad (3)$$

where $P(f)=p(f)\cdot p^{*}(f)$ is the output of the correlator, $\odot$ is the Hadamard multiplication operation, $H^{\mathrm{T}}(f)$ is the response of the T RF chain, $\boldsymbol{H}^{\mathrm{R}}(f)$ is the response of the 64 RF chains, $\boldsymbol{H}(f)$ is the channel response between the T antenna and the R antennas, and $\boldsymbol{N}(f)$ is the system noise. The OTA antenna frequency response follows from (3) as:

$$\widehat{\boldsymbol{Y}}_{\mathrm{OTA}}(f) = \frac{1}{M}\sum_{m=1}^{M}\widehat{\boldsymbol{Y}}^{m}(f;\boldsymbol{H}(f)=A\cdot\mathbf{1}) \quad (4a)$$

$$\approx P(f)\cdot A\cdot H^{\mathrm{T}}(f)\cdot\boldsymbol{W}(f)\odot\boldsymbol{H}^{\mathrm{R}}(f) \quad (4b)$$

where the channel response $\boldsymbol{H}(f)$ is simply the free-space attenuation A of the LoS path given from Friis transmission equation at the T-R distance (3 m). (Note that the attenuation of the LoS path, deliberately expressed as A instead of $A(f)$, is indeed frequency invariant [2][3].) Averaging in (4a) over M samples indexed through m is carried out to virtually eliminate noise, approximated as $\boldsymbol{N}(f)\approx\mathbf{0}$ in (4b); we used M = 128.

The design criteria for the predistortion filter is that the OTA antenna frequency response be equal to the ideal correlation frequency response (multiplied by the free-space attenuation), or

$$\widehat{\boldsymbol{Y}}_{\mathrm{OTA}}(f) = P(f)\cdot A\cdot\mathbf{1}. \quad (5)$$

For convenience, (4b) is rewritten as

$$\widehat{\boldsymbol{Y}}_{\mathrm{OTA}}(f)\approx\boldsymbol{W}(f)\odot\widehat{\boldsymbol{Y}}_{\mathrm{OTA}}(f;\boldsymbol{W}(f)=\mathbf{1}). \quad (6)$$

By equating (5) and (6), the solution for the predistortion filter is given as

$$\boldsymbol{W}(f) = P(f)\cdot A\cdot\mathbf{1}\oslash\widehat{\boldsymbol{Y}}_{\mathrm{OTA}}(f;\boldsymbol{W}(f)=\mathbf{1}), \quad (7)$$

where $\oslash$ is the Hadamard division operator. What remains is to measure the OTA antenna response with no filter $\widehat{\boldsymbol{Y}}_{\mathrm{OTA}}(f;\boldsymbol{W}(f)=\mathbf{1})$, *i.e.* by transmitting the ideal PN code and measuring the OTA response from each of the antennas individually, by switching them on and off sequentially. Fig. 3 shows an example OTA response for one of the 64 antennas for the original predistortion filter design against the ideal response: the frequency response in Fig. 3(a) and the equivalent CIR in Fig. 3(b).

IV. Improved Predistortion Filter

The main issue with the original predistortion filter design – what we discovered only later – is rooted in inadequate isolation between the individual patch antennas on the printed circuit board. Although in the design only a single antenna is active at once, the remaining 63 inactive antennas nevertheless contribute some residual leakage into the Wilkinson power combiner [12] leakage which is in turn summed at the single RF port (per polarization) shared by all antennas. Because the filters are computed separately, the design does not account for the residual leakage. The improved design described in this section does, indeed yielding much better results.

In the improved design, all antennas employ the same filter and so the frequency response in (3) can be simplified by replacing the 64-element row vector $\boldsymbol{W}(f)$ with a single element $W(f)$:

$$\widehat{\boldsymbol{Y}}(f) = P(f)\cdot W(f)\cdot H^{\mathrm{T}}(f)\cdot\boldsymbol{H}(f)\odot\boldsymbol{H}^{\mathrm{R}}(f)+\boldsymbol{N}(f). \quad (8)$$

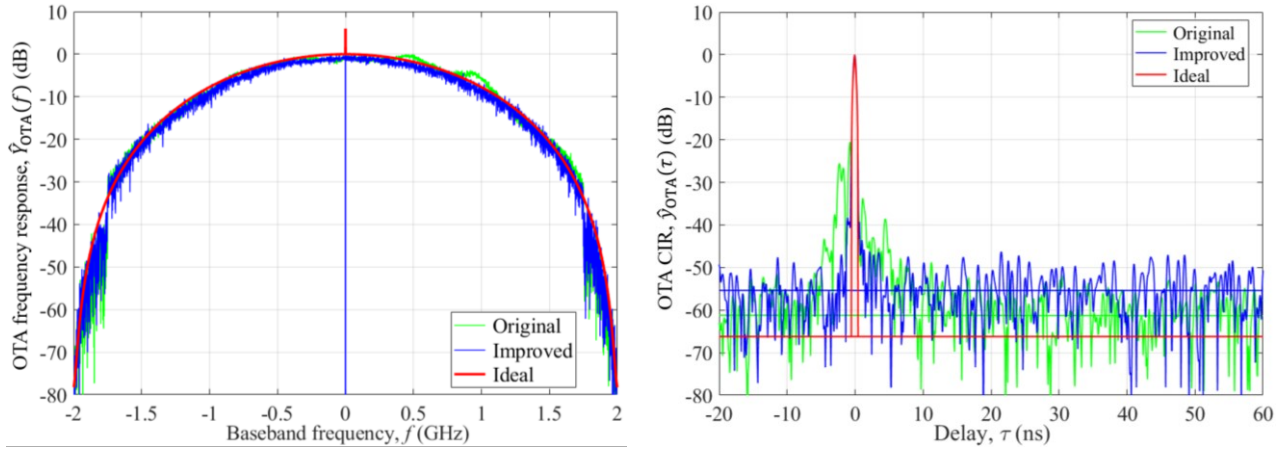

(a) (b)

Figure 3. Comparing the calibrated responses of the original and improved predistortion filters versus the ideal responses. (a) OTA frequency response, $\hat{Y}_{\mathrm{OTA}}(f)$ (b) OTA channel impulse response (CIR), $\hat{y}_{\mathrm{OTA}}(\tau)$

Furthermore, the design is not based on the OTA response from the individual antennas, but rather on OTA response beamformed across all antennas towards the LoS path ($\boldsymbol{\theta} = \mathbf{0}^\circ$) through the calibrated steering vector $\hat{\boldsymbol{s}}(\mathbf{0}^\circ)$:

$$\hat{\boldsymbol{s}}(\mathbf{0}^\circ) \cdot \boldsymbol{Y}_{\mathrm{OTA}}(f)^\dagger = \frac{1}{M}\sum_{m=1}^{M} \hat{\boldsymbol{s}}(\mathbf{0}^\circ) \cdot \boldsymbol{Y}^m(f; \boldsymbol{H}(f) = A \cdot \mathbf{1})^\dagger \quad (9a)$$

$$\approx P(f) \cdot A \cdot H^{\mathrm{T}}(f) \cdot W(f) \cdot \hat{\boldsymbol{s}}(\mathbf{0}^\circ) \cdot \boldsymbol{H}^R(f)^\dagger \quad (9b)$$

The new design criteria is that the OTA beamformed frequency response be equal to the ideal correlation frequency response (multiplied by the free-space attenuation), or

$$\hat{\boldsymbol{s}}(\mathbf{0}^\circ) \cdot \hat{\boldsymbol{Y}}_{\mathrm{OTA}}(f)^\dagger = P(f) \cdot A. \quad (10)$$

Following analogous steps in Section III, (9b) is rewritten as

$$\hat{\boldsymbol{s}}(\mathbf{0}^\circ) \cdot \hat{\boldsymbol{Y}}_{\mathrm{OTA}}(f)^\dagger \approx W(f) \cdot \hat{\boldsymbol{s}}(\mathbf{0}^\circ) \cdot \hat{\boldsymbol{Y}}_{\mathrm{OTA}}(f; W(f) = 1)^\dagger. \quad (11)$$

Then by equating (10) and (11), the solution for the predistortion filter is given as

$$W(f) = \frac{P(f) \cdot A}{\hat{\boldsymbol{s}}(\mathbf{0}^\circ) \cdot \hat{\boldsymbol{Y}}_{\mathrm{OTA}}(f; W(f) = 1)^\dagger}. \quad (12)$$

What remains is to measure the OTA beamformed response with no filter $\hat{\boldsymbol{s}}(\mathbf{0}^\circ) \cdot \hat{\boldsymbol{Y}}_{\mathrm{OTA}}(f; W(f) = 1)^\dagger$, *i.e.* by transmitting the ideal PN code and measuring the OTA response from each of the antennas individually, by switching them on and off sequentially, and then beamforming them into a single response. Fig. 3 also shows the OTA beamformed response using the improved predistortion filter design. In comparison to the original design, the frequency response in Fig. 3(a) is less distorted and much closer to ideal; in the CIR in Fig. 3(b), the peak-to-sidelobe ratio is improved by 21.0 dB.

Unfortunately, the filter design is inextricably coupled to the angle of LoS path in the OTA method, and so any deviation of a path's angle from $\boldsymbol{\theta} = \mathbf{0}^\circ$ will induce a residual phase shift – and in turn residual leakage – across the array, resulting in spurious sidelobes in the CIR that the filter is intended to eliminate. Yet in the field paths may arrive from any angle, and so to mitigate leakage, rather than setting the nominal phase of the analog weights to 0 radians, as described in Section II.B, in the improved design the phases are distributed randomly (while maintaining the nominal magnitude at maximum). Assuming a path's angle in the field will arrive with a uniform distribution, the phases were in kind distributed uniformly across the array antennas (between 0 and 2π) before designing the filter, minimizing the probability that the residual leakage will constructively combine into a high-power sidelobe.

To substantiate the robustness of the improved filter design against different path angles, the OTA setup was modified slightly, by placing the array on a 2D mechanical rotator. The array was then mechanically rotated every 5° across its ±45° azimuth field-of-view and then electronically steered back to alignment with T, effectively varying the azimuth angle θ^{A} of the LoS path to mimic paths in the field. Then the OTA response was measured using the predistortion filter (designed at 0° mechanical rotation). Fig. 4 compares the variation in the response across θ^{A} for the original and improved designs: Fig. 4(a) shows the variation in the CIR's peak-to-sidelobe ratio. While for the improved design, the ratio retracts up to 12.0 dB from 43.6 dB at $\theta^{\mathrm{A}} = 0^\circ$, the average retraction across angle is only 8.4 dB. Most importantly, the ratio is significantly greater for the improved design versus the original design, on average 14.6 dB greater and up to 21.0 dB greater. Not only is the peak-to-sidelobe ratio stable across angle, Fig. 4(b) shows that the peak value in the CIR is even more stable.

V. Future Work

This paper discusses predistortion filtering to calibrate for the hardware imperfections of phased-array antennas that employ switched beamforming for channel sounding. In our

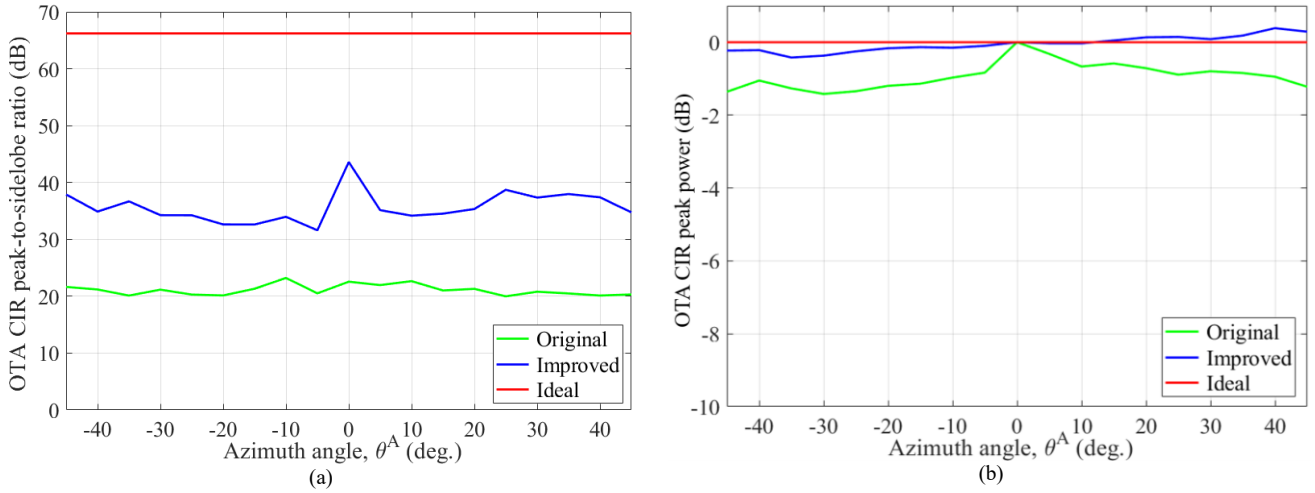

Figure 4. Comparing the variation in OTA channel impulse response (CIR) between the original and improved predistortion filters versus the ideal response, as the beam is steered in azimuth angle away from boresight ($\theta^A = 0°$) (a) Variation in the peak-to-sidelobe of the OTA CIR (b) Variation of the peak power in the OTA CIR (The peak power is normalized to 0 dB at $\theta^A = 0°$ for the original, improved, and ideal CIRs.)

original work, a filter was designed separately for each of the antennas but consequently – as we realized later – did not account for the mutual leakage between the antennas on the printed circuit board. The design proposed in this paper does account for mutual leakage, improving performance, but resolves to a single filter for all antennas. We are currently investigating a design that considers all antennas collectively, but allows for a separate filter for each antenna, exploiting all the degrees of freedom in the design, which should lead to yet improved performance.

REFERENCES

[1] https://nextg.nist.gov

[2] Pi, Zhouyue, and Farooq Khan. "An introduction to millimeter-wave mobile broadband systems." *IEEE Comm. Mag.* 49.6 (2011): 101-107.

[3] Guven, Damla, et al. "Methodology for Measuring the Frequency Dependence of Multipath Channels Across the Millimeter-Wave Spectrum." *IEEE Open J. of Ant. and Propagation* 3 (2022): 461-474.

[4] Salous, Sana, et al. "Millimeter-Wave Propagation: Characterization and modeling toward fifth-generation systems.[Wireless Corner]." *IEEE Ant. and Propagation Magazine* 58.6 (2016): 115-127.

[5] Shafi, Mansoor, et al. "Microwave vs. millimeter-wave propagation channels: Key differences and impact on 5G cellular systems." *IEEE Communications Magazine* 56.12 (2018): 14-20.

[6] Rupakula et al., "63.5-65.5-GHz Transmit/Receive Phased-Array Communication Link With 0.5-2 Gb/s at 100-800 m and±50° Scan Angles." *IEEE Trans. Microw. Theory Techn.*, vol. 66, no. 9, pp. 1-13, Sep. 2018.

[7] Gu, Xiaoxiong, et al. "Development, implementation, and characterization of a 64-element dual-polarized phased-array antenna module for 28-GHz high-speed data communications." *IEEE Trans. Microw. Theory Techn* , 67.7 (2019): 2975-2984.

[8] Chen, Chun-Nien, et al. "38-GHz Phased Array Transmitter and Receiver Based on Scalable Phased Array Modules With Endfire Antenna Arrays for 5G MMW Data Links." *IEEE Trans. Microw. Theory Techn.*, (2020).

[9] Wang, Yaochen, et al. "A 57.5-65.5 GHz Phased-Array Transmit Beamformer in 45 nm CMOS SOI With 5 dBm and 6.1% Linear PAE for 400 MBaud 64-QAM Waveforms." *IEEE Trans. Microw. Theory Techn.*, (2020).

[10] Gao, Li, and Gabriel M. Rebeiz. "A 22–44-GHz Phased-Array Receive Beamformer in 45-nm CMOS SOI for 5G Applications With 3–3.6-dB NF." *IEEE Trans. Microw. Theory Techn.,* 68.11 (2020): 4765-4774.

[11] Caudill, Derek, et al. "Real-time mmWave channel sounding through switched beamforming with 3-D dual-polarized phased-array antennas." *IEEE Transactions on Microwave Theory and Techniques* 69.11 (2021): 5021-5032.

[12] Ma, Qian, et al. "A 5G 24-30 GHz 2x32 Element Dual-Polarized Dual-Beam Phased Array Base-Station for 2x2 MIMO System." *2019 IEEE Global Communications Conference (GLOBECOM)*. IEEE, 2019.

[13] M.F. Akdeniz et al., "Millimeter Wave Channel Modeling and Cellular Capacity Evaluation," *IEEE J. Sel. Areas Comm.*, vol. 32, no. 6, pp. 1164-1179, Jun. 2014.

[14] Hughes, Aidan, et al. "Measuring the Impact of Beamwidth on the Correlation Distance of 60 GHz Indoor and Outdoor Channels." *2021 IEEE Open Journal on Vehicular Technology (OJVT)*. IEEE. 2021.

[15] Cheng, David Keun. "Fundamentals of engineering electromagnetics." (1993).

[16] Högbom, J. A. "Aperture synthesis with a non-regular distribution of interferometer baselines." *Astronomy and Astrophysics Supplement Series* 15 (1974): 417.

[17] Schmidt, Ralph. "Multiple emitter location and signal parameter estimation." *IEEE transactions on antennas and propagation* 34.3 (1986): 276-280.

[18] Roy, Richard, and Thomas Kailath. "ESPRIT-estimation of signal parameters via rotational invariance techniques." *IEEE Transactions on acoustics, speech, and signal processing* 37.7 (1989): 984-995.

[19] Fessler, Jeffrey A., and Alfred O. Hero. "Space-alternating generalized expectation-maximization algorithm." *IEEE Transactions on signal processing* 42.10 (1994): 2664-2677.

[20] Hausmair, Katharina, et al. "SAGE algorithm for UWB channel parameter estimation." *COST 2100 Management Committee Meeting*, 2010.

[21] Richter, Andreas. "Estimation of radio channel parameters: Models and algorithms." ISLE, 2005.

[22] Papazian, Peter B., et al. "Calibration of millimeter-wave channel sounders for super-resolution multipath component extraction." *2016 10th European Conference on Antennas and Propagation (EuCAP)*. IEEE, 2016.

[23] Sun, Ruoyu, et al. "Design and calibration of a double-directional 60 GHz channel sounder for multipath component tracking." *2017 11th European Conference on Antennas and Propagation (EUCAP)*. IEEE, 2017.

[24] Caudill, Derek, et al. "Omnidirectional Channel Sounder With Phased-ArrayAntennas for 5G Mobile Communications." *IEEE Transactions on Microw. Theory Techn.* 67.7 (2019): 2936-2945.

[25] Jun, Sung Yun, et al. "Over-The-Air Calibration of a Dual-Beam Dual-Polarized 28-GHz Phased-Array Channel Sounder." *2020 IEEE International Symposium on Antennas and Propagation and North American Radio Science Meeting*. IEEE, 2020.